Numerical simulation of the 2-D gas flow modified by the action of charged fine particles in a single-wire ESP

Kazimierz Adamiak, Pierre Atten

6ème Conférence de la Société Française d'Electrostatique, Paris & Gif-sur-Yvette, 8-9 juillet 2008, ISBN : 978-2-9505432-6-4, pp. 188-193 (2008)

Numerical Simulation of the 2-D Gas Flow Modified by the Action of Charged Fine Particles in a Single-Wire ESP

Kazimierz Adamiak and Pierre Atten

***Abstract*—A numerical model for simulating precipitation of submicrometer particles in a single-wire electrostatic precipitator is discussed in this paper. It includes all essential phenomena affecting the process: electric field, space charge density, gas flow, including the secondary electrohydrodynamic flow caused by the corona discharge and charged particles, and particle transport. A simplified corona model assumes just one ionic species and neglects the ionization zone. The fully coupled model for the secondary EHD flow, considering the ion convection, has been implemented. The dust particles are charged by ionic bombardment and diffusion. The gas flow pattern is significantly modified by the secondary EHD flow, which depends on the particle concentration. As for fine particles the drift velocity is small and particles practically follow the gas streamlines, the particle concentration has a very strong effect on the precipitation efficiency.**

***Index Terms*—Corona discharge, electrohydrodynamics, electrostatic precipitation, particle charging, fine particles removal**

I. Introduction

While the concept of electrostatic precipitator (ESP) is relatively old and for many years these devices have been used to protect our atmosphere, the whole process is still not completely understood in details. Mutual interaction between an electric field, space charge density, gas flow, its modification by the secondary electrohydrodynamic (EHD) flow and particle transport makes analysis of the entire precipitation process rather complicated. Despite of wealth of literature on this subject the effects of different factors and criteria for optimum precipitator configurations continue to be a subject of discussion and sometimes contradicting conclusions.

Manuscript received April 30, 2008. This work was supported in part by CNRS (trough invitation of K.A. in GE2 Lab) and the Natural Sciences and Engineering Research Council (NSERC) of Canada.

K. Adamiak is with the Department of Electrical and Computer Engineering, University of Western Ontario, London, Ontario, Canada N6A 5B9 (phone: 519-661-2111 ext.88358; fax: 519-850-2436; e-mail: kadamiak@eng.uwo.ca).

P. Atten is with G2Elab, a laboratory common to French CNRS, Joseph Fourier University and Institute of Technology of Grenoble, CNRS site : 25 av. des Martyrs, Grenoble, France (phone: +33 476 88 11 71, Fax: +33 476 88 79 45, e-mail: pierre.atten@grenoble.cnrs.fr).

One of the first interesting issues was the electrohydrodynamic origin of turbulence in ESPs [1]. Action of the electric field on the space charge results in the Coulomb force producing gas motion, which, in turns, affects the charge transport. This effect can lead to a much more intense turbulence than caused due to an interaction with the precipitation walls. Increased turbulence changes aerodynamic conditions in the precipitation channel and, according to many researchers, is detrimental to the particle transport [2]. However, some initial research results also seem to indicate improvement in the precipitation efficiency due to the EHD flow under certain conditions [3].

Numerical simulation is a natural choice for investigating the effect of different factors on the precipitation efficiency. Yamamoto and his co-workers have clearly been the leaders in this field. Even though their corona discharge models were quite simplistic, it was emphasized from the very beginning that non-uniform electric field and gas flow distributions are crucial for the complete description of particle transport. As the negative corona discharge occurs in the form of discrete tufts, it was necessary to consider 3-D models of the process, even for smooth discharge electrodes [4]. Improved models of the same authors presented later [5] still accepted some common idealizing assumptions, for example the point charge injection zone and negligible ion convection, but were able to show detailed 3-D distributions of potential, electric field, space charge and secondary gas flow for the two-wire and four-wire ESP geometries. Severe interaction between primary and secondary flows was observed with pairs of spiral vortices formed between the corona tufts in the direction of the gas flow.

The effect of secondary EHD flow depends of course on the primary flow magnitude: the size of spiral rings is reduced by the increased primary velocity. Similar investigations were subsequently performed for barbed-electrode multi-wire precipitators [6] and for turbulent flow models [7]. It has been observed that the distance between spikes is critical for the flow pattern: for larger distances a well-organized spiral flow is formed, while at the reduced distance a turbulent flow arises. These agreed with the earlier experimental observations: for the positive corona discharge, which is uniform along the corona wire, the flow turbulence increases only slightly whereas the negative corona discharge strongly reinforces the turbulence intensity [8,9].

A very detailed study of the effect of secondary EHD flow on the overall flow pattern in the electrostatic precipitator was presented by Soldati [10], who investigated 3-D, time-dependent, fully developed channel flow interacting with the EHD vortices. The corona model was again rather simple, as the Finite Difference discretization was not able to accurately represent the ionic transport close to the discharge wires. However, Direct Numerical Simulation (DNS) technique provided a very clear picture of the flow field, which was examined using a triple decomposition into a mean field, an organized EHD flow and a turbulent flow. It has been confirmed that pairs of counter-rotating EHD vortices are advected downstream by the main flow. Continuing his research, the same author also examined the particle transport and deposition in the wire-plate precipitator by performing Lagrangian simulation of particle trajectories [11]. The final conclusions were rather surprising, indicating that the EHD flow has a negligible influence on the overall particle collection efficiency: EHD flow contributes to a particle re-entraining in the central region of the channel, but also sweeps them towards the walls in other regions.

The numerical model of the secondary EHD flow in ESP presented in [12] focused on accurate prediction of the charge transport. All calculations were performed for a 2-D turbulent flow model assuming infinitely long discharge wires and collection plates, but the fine discretization of the corona wire area made it possible to predict the total ionic current for a given wire voltage. The ionic drift was simulated using the Method of Characteristics, which is immune to the numerical diffusion and can easily incorporate the ion convection. Detailed analysis of different external flow and wire voltage levels revealed that at least eight flow patterns are possible. Recent experimental investigations using the method of Particle Image Velocimetry (PIV) confirmed a significant interaction between the electric field, space charge and flow fields [13].

Collection efficiency of the conventional ESPs is usually satisfactory for large particles, but is much poorer for sub-micron particles. The drift velocity of such particles is small and they practically follow the gas streamlines [14]. In this situation the effect of secondary EHD flow is much more pronounced. What is more important, the charged particles can significantly contribute to the magnitude of EHD flow. Experimental investigations published in [15] indicate that the mean values of the dust and ionic space charge densities can be comparable. In this situation the flow velocity and the level of its turbulence strongly depend on the dust density, especially in the region close to the corona wire.

This paper presents the results of numerical investigations of the gas flow and particle trajectories in a simple two-dimensional model of ESP. The problem is simulated using a hybrid numerical algorithm, in which the electric field is calculated using the Finite Element Method, the ion drift by the Method of Characteristics and the gas flow by the Finite Volume Method. The flow simulation is done in the FLUENT commercial software, with other parts coded as the User Defined Functions.

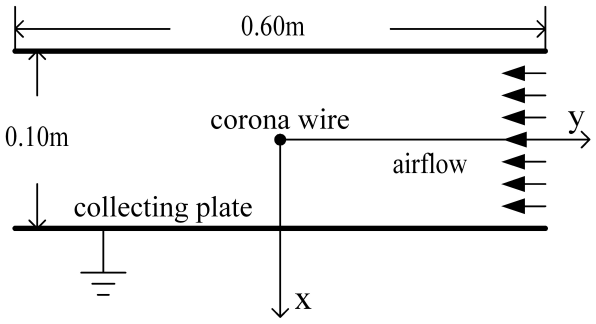

Fig. 1. Schematic configuration of the investigated precipitator.

I. Precipitator Model

As most of industrial ESPs are the wire-plate devices, this model is investigated in the paper. A single discharge electrode (cylindrical wire) is located symmetrically between two collecting plate electrodes (Fig.1). Gas flows in the direction parallel to the ground plates, but is modified by the ionic wind. Neutral sub-micron particles, with spherical shape, are injected at the precipitator entrance and are charged by the field and diffusion charging as they move along the channel and cross the ionic space charge zone. Affected by the electric and aerodynamic forces some of these particles are deposited on the walls, while others exit the precipitation channel on the other side. The deposited particles are removed from the model and they don't contribute to the electric field distribution or to the flow pattern.

II. Mathematical Model

A. Electric Field and Space Charge

A simple single-species stationary corona discharge model is implemented in this paper. The ionization layer is neglected and just one ionic species is injected from the corona electrode surface. These ions drift with an average mobility until they are deposited on the surface of the grounded electrodes. The mathematical description involves the equations for the electric potential and current continuity

$$\nabla^2 \Phi = -\frac{q_i + q_p}{\varepsilon_0} \tag{1}$$

$$\nabla \cdot ((k_i \vec{E} + \vec{u}) q_i + (k_p \vec{E} + \vec{u}) q_p) = 0 \tag{2}$$

where Φ (V) is the electric potential, q_i (C/m^3) – space charge density of ions, q_p (C/m^3) – space charge density of particles, ε_0 (F/m) – ambient gas permittivity, k_i (m^2/Vs) – ion mobility, k_p (m^2/Vs) – particle mobility, $\vec{u}$ (m/s) – vector of gas velocity and $\vec{E} = \nabla \Phi$ – the electric field vector. Eq. (2) is valid assuming that the ion diffusion can be neglected.

Formulation of the boundary conditions is trivial for the potential Φ: the surfaces of corona wire and ground plates are equipotential (Dirichlet conditions). No exact boundary condition can be specified for the channel inlet and outlet.

However, these parts are sufficiently far from the most critical region around the corona wire, so zero normal derivative of the electric potential (homogeneous Neumann conditions) is usually sufficiently accurate.

The boundary conditions for the space charge are more problematic. As the ionization layer has been neglected in this model, exact formulation of these boundary conditions is not possible. Kaptzov's hypothesis is usually accepted, stating that for voltages above the onset level the electric field remains constant at the value given by the empirical Peek's formula

$$E_0 = 3.1 \cdot 10^6 (1 + \frac{0.308}{\sqrt{0.5 \cdot r}}) \tag{3}$$

where r is the corona wire radius in cm. While this formula is theoretically valid for 1-D wire-cylinder geometry, where the electric field on the corona wire surface is constant, it has been proved [16] that accuracy of the simulation is preserved for non-uniform electric fields, too. The charge transport equation (2) is of the first order, so that no boundary condition is needed on other domain boundaries.

B. Gas flow

Under the assumption of incompressible ambient air, the gas has constant density and viscosity; the air flow has to satisfy the continuity and the conservation of momentum equations [12]:

$$\nabla \cdot \vec{u} = 0 \tag{3}$$

$$\rho_f [\frac{\partial \vec{u}}{\partial t} + (\vec{u} \cdot \nabla)\vec{u}] = -\nabla P + \eta \nabla^2 \vec{u} + \vec{F} \tag{4}$$

where ρ_f (kg/m^3) is the gas density, P (Pa) - the static pressure, η (kg/m·s) - the air viscosity, and $\vec{F}$ (N/m^3) - the body force, in this case equal to the Coulomb force $\vec{F} = (q_i + q_p)\vec{E}$.

The flow velocity vector $\vec{u}$ must vanish on all solid surfaces (corona electrodes and channel walls); it takes a specific profile at the channel inlet and the pressure at all points of the outlet has the same value.

C. Particle Concentration

The particles injected into the precipitation channel are assumed to be spherical, to be electrically neutral and to move with a uniform initial velocity equal to the gas velocity. As soon as they enter the region where the ionic space charge exists, they become electrically charged. There are two mechanisms responsible for imparting charge onto the particles: field charging (ionic bombardment) and diffusion charging.

The first effect occurs only if the actual particle charge Q_p is smaller than the saturation charge Q_s, given by the formula

$$Q_s = \frac{2\varepsilon}{\varepsilon + 2} \pi \varepsilon_0 d_p^2 E \tag{5}$$

where ε is the particle relative permittivity. Diffusion charging can occur even for Q_p above the saturation level, but its practical contribution is most often minimal. The overall charging rate is given as [17]:

$$\frac{dQ_p}{dt} = \begin{cases} \frac{Q_s}{\tau_q}(1 - \frac{Q_p}{Q_s})^2 + \frac{2\pi\alpha\rho\, kk_B T d_p}{e} & \text{for} \quad Q_p < Q_s \\ \frac{\alpha}{4\tau_q}(Q_p - Q_s)\exp(\frac{e(Q_s - Q_p)}{2\pi\varepsilon_0 kk_B T d_p}) & \text{for} \quad Q_p > Q_s \end{cases} \tag{6}$$

where

$$\alpha = \begin{cases} 1 & e_{norm} < 0.525 \\ \frac{1}{(e_{norm} + 0.457)^{0.575}} & e_{norm} > 0.525 \end{cases}$$

$$e_{norm} = \frac{e d_p}{2 k_B T}\left|\vec{E}\right|, \qquad \tau_q = \frac{4\varepsilon_0}{k\rho}$$

τ_q being the charging time constant, k_B – Boltzmann coefficient and T – temperature.

A moving particle experiences inertial, air drag and electrical forces. All are balanced in the Newton equation, which needs to be solved in order to determine the particle trajectory. For sub-micrometer particles, inertia is very small and can be neglected. In this situation, the so-called particle migration velocity can be calculated first

$$\vec{v}_d = \frac{Cu \cdot Q_p}{3\pi\eta d_p}\vec{E} \tag{7}$$

where Cu is the Cunningham factor, calculated as

$$Cu = 1.0 + 1.246\frac{2\lambda_g}{d_p} + 0.42 * \frac{2\lambda_g}{d_p}\exp(-0.435 * d_p / \lambda_g)$$

$\lambda_g = 6.5\ 10^{-8}$ m – the mean free path of the gas molecules.

When the migration velocity is known, the particle trajectory is calculated by a simple integration

$$\frac{\partial \vec{x}_p}{\partial t} = \vec{u} + \vec{v}_d \tag{8}$$

where $\vec{x}_p$ – is a vector defining particle position along the trajectory.

III. Numerical Algorithm

The numerical algorithm is based on the Finite Element Method (FEM) and FLUENT flow dynamics commercial software. The whole domain is discretized into approximately 9500 triangular elements distributed in a very non-uniform way with smallest elements close to the corona wire and much larger elements near the inlet and outlet of the precipitation channel. The laminar flow model has been assumed and the Navier-Stokes equation (4) is solved in time domain by FLUENT. The electric body force has to be determined separately using so-called User-Defined-Functions (UDF). Before this is done the electric field and space charge distributions are determined. This is done in another UDF,

which is based on FEM for the electric field and on the Method of Characteristics for the space charge. A double iterative loop is employed, in which the space charge density on the corona wire surface and in the entire precipitation space is iterated until convergence is reached for all involved variables. The corona model includes the convection current, as far from the corona wire, it can visibly modify the ion trajectory and the space charge density [12].

A given number of spherical particles are injected at every time step from the channel inlet. All of them are electrically neutral and have the same size and initial velocity. They start from uniformly distributed rectangular cells with random initial particle position inside of each cell. The super-particle approach is used, in which each particle moves as a single particle with real parameters. However, this super-particle carries a charge of some number of particles. The particle distribution is sufficiently dilute, so they do not affect the air velocity field. The particle charge is calculated by integrating the charging equation (6).

IV. Results and Discussion

The above numerical algorithm has been applied for simulating a single-wire EPS precipitator, assuming that the diameter of corona wire is 1 mm, collecting plates are 10 cm apart, average gas velocity at the inlet is 0.4 m/s and 30 kV is applied to the corona wire. Injected dust particles are spherical in shape with the diameter of 0.3 μm. Their concentration is expressed in terms of the reference value of $c_0 = 2 \cdot 10^{+12}$ particles/m^3.

A. Electric Field and Space Charge

Electric potential distribution follows an expected pattern: close to the equipotential wire the equipotential lines are practically circular. Large concentration of lines indicates strong electric field in this area. The lines deform as the distance to the corona wire increases showing an oval shape. Eventually, the equipotential line becomes completely flat at the ground plate.

Gas ionization occurs in a thin corona sheet surrounding the corona wire. The maximum space charge density in this region is about 190 μC/m^3, but this density sharply decreases towards the ground plate. Close to the inlet and outlet of the precipitation channel the space charge density decreases to a very small value.

B. Flow Velocity Streamlines

Without the action of electrical forces the gas flow follows regular laminar path lines shown in Fig. 2a. Depending on the Reynolds number, von Karman vortices can be created behind the corona wire, but they are too small to be visible. When the wire voltage is above the corona onset level, the corona discharge generates the secondary EHD flow. Without external flow four doubly symmetrical vortices are created [12]. The presence of charged dust particles also contributes to the generation of EHD flow, but this pattern is not symmetric with respect to the vertical plane: upstream the corona wire the particles are not fully charged yet, so in this region the electric body force is much smaller than in the downstream region, where the particles are fully charged and much stronger EHD flow can be expected. The final flow distribution results from the balance of all three components.

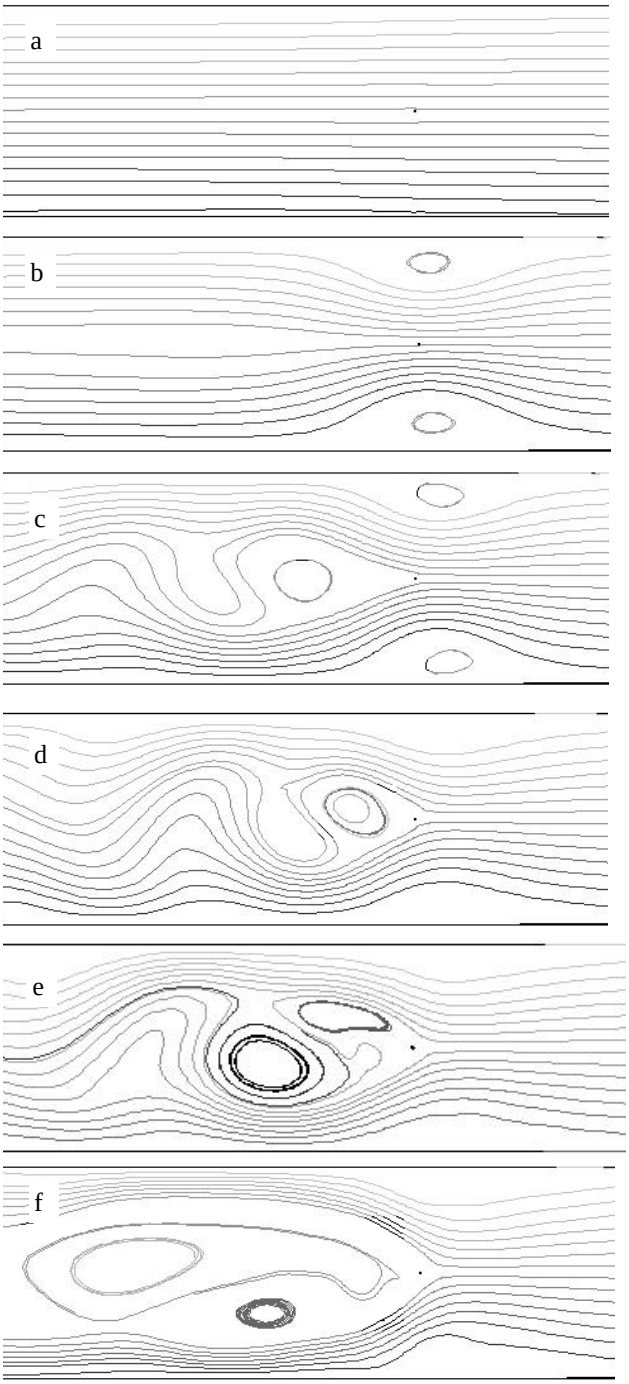

Fig. 2 Gas path lines for different dust particle concentrations (corona wire voltage equal to 30 kV, input gas velocity 0.4 m/s).
a). no corona discharge, $c = 0$, b).corona discharge, $c = 0$, c). corona discharge, $c = c_0$, d). corona discharge, $c = 8c_0$, e). corona discharge, $c = 12\ c_0$, f). corona discharge, $c = 20\ c_0$.

Without the presence of charged dust particles the flow

pattern is practically dominated by the external gas flow (Fig. 2b). The two upwind vortices generated by the corona discharge are shifted towards the walls and two downwind vortices are squeezed towards the channel plane of symmetry forming an elongated wake.

The charged dust presence dramatically changes aerodynamic conditions in the channel: time dependent vortices grow in size with increased particle concentration until they eventually occupy the major part of the channel downstream the corona wire (Fig. 2e). The flow is not steady and it exhibits violent oscillations.

C. Particle Concentration

Fig.3 shows the dust particle distribution for different dust densities. As expected, the dust particles are mostly affected by the air drag force with a rather weak contribution of the electric force. When the dust concentration is very small (Fig. 3a) the particle charge doesn't affect the flow pattern and particle trajectories basically follow the gas streamlines shown in Fig. 2b. The dust particles are swept from the area of two upwind vortices. Also, a thin trail downwind of the corona wire exists, where the dust particles are removed by the electric force. Increased dust concentration changes the flow structure and the dust concentration pattern.

With an increased dust concentration the region with the negligible particle concentration spreads out towards the collecting plates, what can be seen as a factor improving the dust collection, because the particles are driven towards the collecting plates. However, vortex formation downwind the corona wire drives the dust particles again towards the channel centre. This kind of flow might even re-entrain particles already deposited on the walls. The particle re-entrainment is not included in the presented algorithm; so calculated values of the deposition efficiency improve with the dust concentration. This is contrary to the experimental observations, where the collection efficiency is actually deteriorated, when the dust concentration is increased [18].

D. Voltage-current characteristics

The presence of charged dust particles influences the corona discharge. The dust-generated space charge adds to the ionic space charge. As the total space charge produces the same effect on the electric field on the wire, an increase in dust concentration reduces the ions concentration and, therefore, the total corona current under the same voltage [15].

Numerical simulations confirm this picture (Fig. 4). Under 30 kV, without dust the total corona current is $I \cong 200$ μA; this current decreases with c and at $c = 20\ c_0$ we obtain $I \cong 120$ μA, i.e. a reduction of about 40 %. This estimate fairly well agrees with measurements presented in [15], although exact comparison of the concentration levels is not possible, as in the experiments the dust has a poly-dispersed size distribution.

E. Charging level of dust particles

The dust particles are charged mainly by the field charging with a small addition by the diffusion charging. The charging level is a function of the maximum electric field the particle

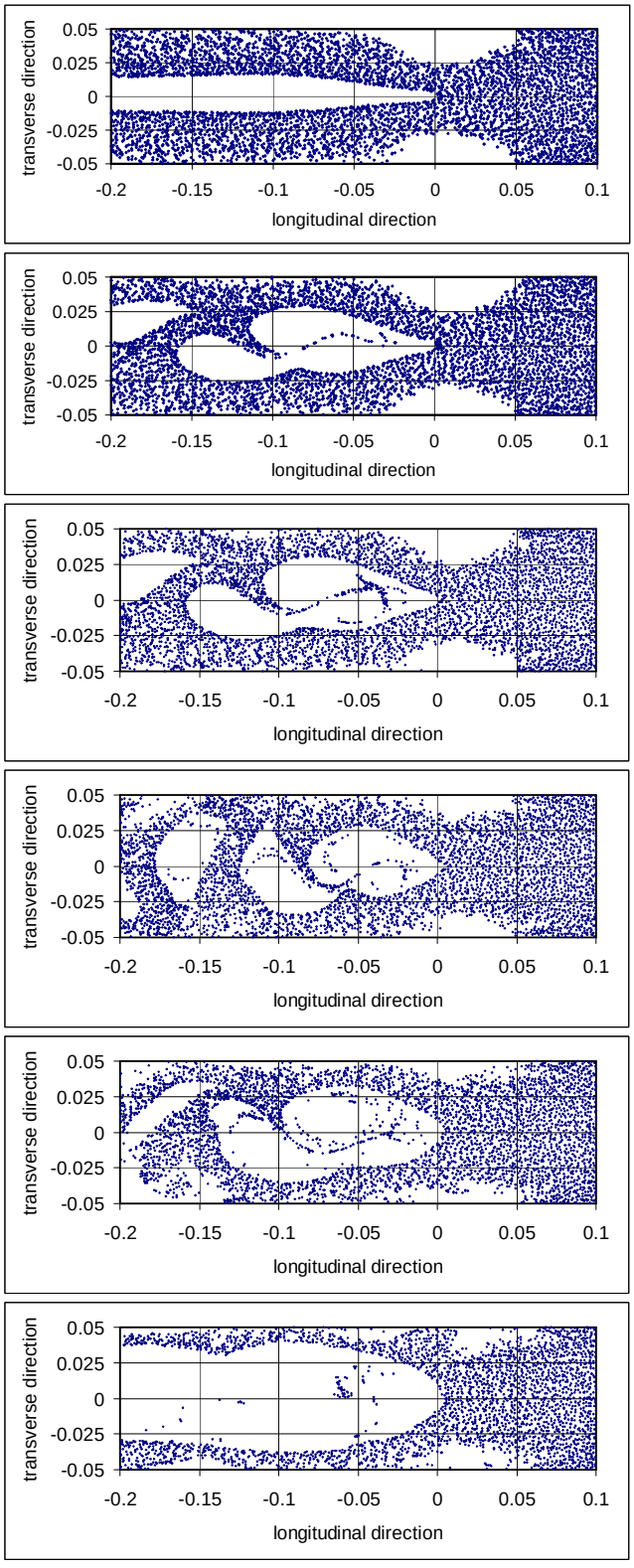

Fig. 3 Dust particle pattern for different dust particle concentrations (corona wire voltage equal to 30 kV, input gas velocity 0.4 m/s).
a) $c \approx 0$, b) $c = 0.2\ c_0$, c) $c = c_0$, d) $c = 8\ c_0$, e) $c = 12\ c_0$, f). $c = 20\ c_0$

has been exposed to; therefore, different particles are charged differently depending on their trajectories: those passing in close proximity of the corona wire are charged to a much

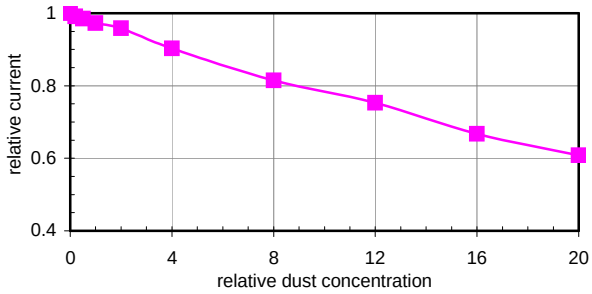

Fig. 4 Corona current versus dust concentration
(corona wire voltage – 30 kV, gas velocity – 0.4 m/s)

higher level than the ones migrating close to the collecting walls.

Fig. 5 shows examples of the dust charge distribution both for the collected and uncollected particles. It may be first surprising to see that the uncollected particles are charged to a much higher level than the collected ones. However, it is obvious that the electric forces play a minor role in the dust precipitation: collected particles were injected close to the wall and were deposited by the mechanical forces: migrating close to the ground electrodes they were exposed to a weak electric field and didn't gain significant electric charge. There are two humps on this graph: the first one corresponds to precipitation in the area of upwind vortices, the second one – to precipitation in the area downwind the corona wire.

V. Conclusions

The results presented in the paper show the effect of particle concentration on the gas flow streamlines, on the particle distribution pattern and on the current-voltage characteristics of the single-wire ESP. Increasing the particle concentration significantly affects the flow pattern which becomes more and more non-uniform and exhibits stronger and stronger agitation. Increasing the particle concentration also increases the space charge due to particles, what results in a reduction of the corona current. Obtained results qualitatively agree with the experimental data [15].

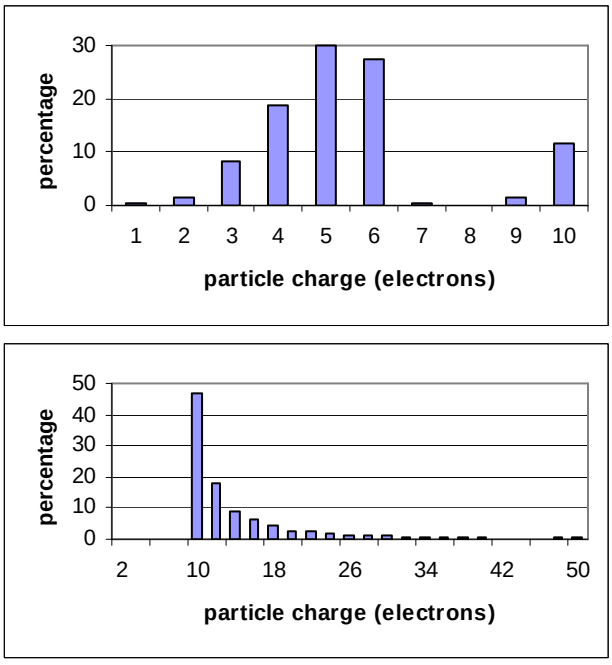

Fig. 5 Charge distribution of the collected (a) and uncollected (b) particles (particle density $c = 0.2\ c_0$)

References

[1] P. Atten, F.M.J. McCluskey and A.C. Lahjomri, "The electrohydrodynamic origin of turbulence in electrostatic precipitators," *IEEE Trans. Ind. Appl*., vol. 23, pp.705-711, July/Aug. 1987.

[2] J.H. Davidson and P.J. McKinney, "EHD flow visualization in the wire-plate and barbed plate electrostatic precipitator," *IEEE Trans. Ind. Appl*., vol. 27, pp. 154-160, 1991.

[3] R.S. Withers and J.R. Melcher, "Augmentation of single-stage electrostatic precipitation by electrohydrodynamic instability," *Ind.Eng.Chem.Res*., vol.27, pp.170-179, 1988.

[4] T. Yamamoto and L.E. Sparks, "Numerical simulation of three-dimensional tuft corona and electrohydrodynamics," *IEEE Trans. Ind. Appl*., vol. 22, pp. 880-885, 1986.

[5] T. Yamamoto, M. Okuda and M. Okubo, "Three-dimensional ionic wind and electrohydrodynamics of tuft/point corona electrostatic precipitator,", *IEEE Trans. Ind. Appl*., vol. 39, pp. 1602-1607, 2003.

[6] H. Fujishima, Y. Morita, M. Okubo and T. Yamamoto, "Numerical simulation of three-dimensional electrohydrodynamics of spiked-electrode electrostatic precipitators,", *IEEE Trans. Dielect. Electr. Insul*., vol. 13, pp. 160-167, 2006.

[7] T. Yamamoto, Y. Morita, H. Fujishima and M. Okubo, "Three-dimensional EHD simulation for point corona electrostatic precipitator based on laminar and turbulent models," *J. Electrostat*., vol. 64, pp. 628-633, 2006.

[8] G.L. Leonard, M. Mitchner and S.A. Self, "An experimental study of the electrohydrodynamic flow in electrostatic precipitators," *J. Fluid Mech*., vol. 127, pp. 123-140, 1983.

[9] G.A. Kallio and D.E. Stock, " Interaction of electrostatic and fluid dynamic fields in wire-plate electrostatic precipitator," *J. Fluid Mech*., vol. 240, pp. 133-166, 1992.

[10] A. Soldati, "Turbulence modification by large-scale organized electrohydrodynamic flow," *Phys.Fluids*, vol. 10, pp. 1742-1756, 1998.

[11] A. Soldati,"On the effects of electrohydrodynamic flows and turbulence on aerosol transport and collection in wire-plate electrostatic precipitators," *J. Aerosol Sci*., vol. 31, pp. 293-305, 2000.

[12] L. Zhao and K. Adamiak, "Electrohydrodynamic flow in a single wire-plate electrostatic precipitator," in *Proc. ESA/IEJ/IEEE-IAS/SFE Joint Conf. Electrostat*., Berkeley, 2006, vol. 2, pp. 763-772.

[13] J. Podlinski, J. Dekowski, J. Mizeraczyk, D. Brocilo and J.-S. Chang, "Electrohydrodynamic gas flow in a positive polarity wire-plate electrostatic precipitator and the related dust particle collection efficiency," *J. Electrostat*., vol. 64, pp. 259-262, 2006.

[14] L.M. Dumitran, P. Atten and D. Blanchard, "Numerical simulation of fine particles charging and collection in an electrostatic precipitator with regular barbed electrodes,", in *Inst. Phys. Conf. Ser*. No. 178, pp. 199-205, 2003.

[15] J. Podlinski, A. Niewulis, J. Mizeraczyk and P. Atten, "ESP performance for various dust densities," *J. Electrostat*., vol. 66, pp. 246-253, 2008.

[16] K. Adamiak, V. Atrazhev and P. Atten, "Corona discharge in the hyperbolic point-plane configuration: direct ionization criterion versus approximate formulations," IEEE Trans. Diel. Electr. Insul., vol. 12, pp. 1025-1034, 2005.

[17] Lawless P.A. & Sparks L.E., Modeling particulate charging in ESPs. IEEE Trans. Ind. Appl., vol. IA24, N° 5, pp. 922-927, 1988.

[18] P. Atten, H.L. Pang, J.-L. Reboud, J. Podlinski and J. Mizeraczyk, "Turbulence generation by charged fine particles in electrostatic precipitators and its effect on collection efficiency", submitted to *J. Electrostat*..